Electron Spin−Echo Envelope Modulation Study of Multicrystalline Cu^{2+}-Insulin: Effects of Cd^{2+} on the Nuclear Quadrupole Interaction of the Cu^{2+}-Coordinated Imidazole Remote Nitrogen†

Michael J. Colaneri,*,‡,§ Jacqueline Vitali,|| and Jack Peisach§

Department of Chemistry and Physics, State University of New York at Old Westbury, Old Westbury, New York 11568, Department of Physiology and Biophysics, Albert Einstein College of Medicine, 1300 Morris Park Avenue, Bronx, New York 10461, and Department of Chemistry, Boston College, Chestnut Hill, Massachusetts 02167

Received July 13, 1999; Revised Manuscript Received November 1, 1999

ABSTRACT: A comparison of electron spin−echo envelope modulation (ESEEM) spectra from multicrystalline Cu^{2+}-insulin with and without additional Cd^{2+} show a dramatic change in the quadrupole coupling parameters of the remote nitrogens of the two histidine imidazoles that ligate to copper. Without Cd^{2+}, the quadrupole parameters are like those observed in blue copper proteins and in copper substituted lactoferrin. With Cd^{2+} soaked into the Cu^{2+}-insulin crystals, the quadrupole parameters are similar to those found in galactose oxidase. Theoretical simulations of ESEEM spectra guided by structure modeling suggest that these changes originate from differences in the hydrogen bonding environments of the imidazole remote nitrogen. In addition, a compilation of results from previous ESEEM studies of copper proteins reveals that the asymmetry parameter, η, may be an indicator of type of hydrogen bond the imidazole remote nitrogen makes. When $\eta \geq 0.9$, the nitrogen hydrogen bonds to water, whereas when $\eta < 0.9$, the nitrogen hydrogen bonds to the protein.

Since first utilized in investigations of proteins possessing a paramagnetic metal ion, ESEEM[1] has been a powerful and useful probe of the electronic environment of distant nuclei, based on the examination of nuclear quadrupole and hyperfine coupling parameters (*1*). For ^{14}N nuclei weakly coupled to Cu^{2+}, as found in the remote ^{14}N of ligated imidazole, the quadrupole parameters e^2qQ/h and η are readily obtained as they fulfill the experimental requirement for observing a strong ESEEM effect known as "exact cancellation" (*2, 3*). This is where the hyperfine coupling equals twice the nuclear Larmor frequency, resulting in the approximate nuclear quadrupole resonant condition in one of the electron spin manifolds and in the ESEEM spectrum (*2, 3*). The nuclear quadrupole interaction is of particular interest because it gives information about the electric field gradient at the nucleus, and is therefore a probe of the surrounding electronic charge distribution. Other spectral parameters are the isotropic and anisotropic components of the hyperfine tensor and the orientation of the principal axes for these tensors. These describe the interaction between electron and nuclear spins and provides a measure of the extent of electron spin delocalization. In addition, combinations of modulation frequencies become apparent in the ESEEM decay patterns when more than one nuclear coupling exists (*4*−*7*). A careful analysis of the ESEEM spectra obtained by Fourier transformation of the electron spin−echo decay envelopes has therefore given both quantitative and qualitative measures of the interactions of imidazole remote nitrogens in many copper-containing model systems and metalloproteins (*8*).

Both natural and artificial copper proteins have been studied over the years by ESEEM and other related techniques. The results obtained have been used to formulate a hypothesis concerning the magnitude of the quadrupole coupling interaction for the remote ^{14}N of coordinated histidine imidazole. That is, variations in the nqi parameters for the remote nitrogen in copper proteins are attributable to differences in hydrogen-bonding interactions (*9*−*11*).

For type 1 copper sites, as found in all blue copper proteins, there is always a remote nitrogen atom of one of the two imidazole ligands to the metal ion that is hydrogen-bonded to a carbonyl oxygen from the backbone or a side chain, based on X-ray crystallography (*12*−*21*). The second coordinating histidine imidazole has been found, in some cases, to have its remote ^{14}N hydrogen-bonded to a structured water molecule. However, this water has not always been detected, and here, no other hydrogen-bond interaction is evident. An exception appears in cucumber stellacyanin, where both coordinating imidazoles have their remote

† This work was supported by a Cottrell College Science Award (CC4518) from Research Corporation, by NIGMS MBRS Grant 3S06GM08180-17S2, and by New York State (GRI) to M.J.C., and by U.S. Public Health Service Grants RR-02583 and GM-40168 to J.P.

* To whom correspondence should be addressed: phone (516) 876-2756; e-mail mike@EPR2.oldwestbury.edu.

‡ State University of New York at Old Westbury.

§ Albert Einstein College of Medicine.

|| Boston College.

[1] Abbreviations: ESEEM, electron spin−echo envelope modulation; FT-ESEEM, Fourier-transformed electron spin−echo envelope modulation; ESE, electron spin−echo; EPR, electron paramagnetic resonance; nqi, nuclear quadrupole interaction; e^2qQ/h, maximum quadrupole coupling; η, quadrupole asymmetry parameter; a_{iso}, isotropic hyperfine component, ν_n, ^{14}N nuclear Larmor frequency, A^{Cu}, copper hyperfine interaction.

10.1021/bi991613v CCC: $19.00
Published on Web 12/28/1999

nitrogens hydrogen-bonded to water molecules (*22*). Interest in the solvent-exposed coordinated histidine imidazole comes from propositions on the mechanisms of action of the copper proteins, azurin and ascorbate oxidase. For example, results derived from the crystal structures of His35Gln and His35Leu azurin mutants prompted Nar et al. (*23*) to suggest that it is the solvent-exposed imidazole and the water molecule specifically hydrogen-bonded to the remote nitrogen of this imidazole that are the conduit for electron transfer between the copper site and the protein's natural redox partners.

To more fully examine the relationship between the hydrogen-bonding interaction of the remote nitrogen of histidine imidazole and the quadrupole coupling parameters, with special interest in systems where the remote imidazole nitrogen is hydrogen-bonded to water, the present ESEEM investigation of multicrystals of Cu^{2+}-substituted porcine Zn^{2+}-insulin was initiated.

Insulin is a small (51amino acid) hormone important for regulating the cellular uptake of glucose and which, over longer time periods, is necessary for normal cell growth and proliferation (*24*). This protein readily crystallizes in the presence of divalent ions (*25, 26*), such as Zn^{2+}, Cd^{2+}, Co^{2+}, Ni^{2+}, Cu^{2+}, Mn^{2+}, or Fe^{2+}. Zinc-insulin (referred to as 2Zn-insulin) crystals have rhombohedral space group *R*3, with two zinc ions and six monomers per unit cell (*27, 28*). The crystal symmetry requires that this hexamer be organized as three equivalent dimers related to each other by a 3-fold rotation. The dimer constitutes the asymmetric unit. Perpendicular to the 3-fold axis, there is a noncrystallographic 2-fold axis of symmetry that relates the two monomers of the dimer, and also two dimers of the hexamer (*28*). The two zinc atoms are ≈16 Å apart and situated on the 3-fold crystal axis. These have slightly different environments, due to the slightly different monomer conformations in the dimer. The coordination of each zinc ion consists of three histidine (His B10 or His D10) imidazole nitrogens (Nϵ) and three waters (OW). At the center of the 2Zn-insulin hexamer, six glutamate (Glu B13) side chains and water molecules cluster together. A network of hydrogen bonds links these Glu side chains with each other and with the imidazole of metal-coordinated His B10 (or His D10) via ordered water molecules. The (His B10, His D10)N$\delta\cdots$ OW$\cdots$ (Glu B13)Oϵ hydrogen-bond distances are ≈3 Å and ≈2.7 Å, respectively (*28*).

Single crystals of porcine 2Cu-insulin has been the focus of a previous EPR study by Brill and Venable (*29, 30*), who were able to determine the **g** and copper hyperfine tensors for two closely similar copper sites, A and B. In their pioneering study, these authors also performed X-ray precession experiments on 2Zn-insulin as well as 2Cu-insulin (*29*). Conclusions drawn from their work were the following; (1) the crystal structure of the copper and zinc insulins is essentially the same, (2) there are two distinct, but similar, metal binding sites per hexamer, (3) the metal is bound on the trigonal axis, (4) the EPR rotational pattern and tensor parameters show two sets of three copper absorptions, each related by the 3-fold crystal axis, and therefore one set for each metal site, (5) the EPR results indicate that each copper is bound on a statistical trigonal axis due to Jahn−Teller distortions, and (6) the copper is six-coordinate possessing two histidine imidazole nitrogens and two water molecules in a very approximate equatorial plane, with a third histidine imidazole nitrogen and water bound axially at a further distance. These conclusions were either confirmed or found to be consistent with the accurate 2Zn-insulin structure that was later reported (*28*).

In the present study, small crystals of Cu^{2+}-insulin were grown and multicrystalline samples were studied by EPR and pulsed-EPR spectroscopies. The EPR spectrum for Cu^{2+}-insulin was changed when Cd^{2+} was allowed to soak into the crystals. Previous crystallographic studies on Cd^{2+}-insulin revealed that, in addition to the cadmium substituting for the two zinc atoms, another cadmium binds to two glutamate (Glu B13) side chains that occur at the hexamer interface (*31*). The presence of this cadmium was reported to only cause a local disturbance of the Glu B13 residue conformations, as the remaining insulin structure was found to be identical to that in 2Zn-insulin. On the other hand, EPR and three-pulse ESEEM spectra of Cu^{2+}-insulin exhibit a significant change upon Cd^{2+} binding. Analysis of these results indicate a slight rearrangement of the copper site as well as a change in the nqi parameters of the imidazole remote nitrogens. These changes are attributed to a specific alteration in the insulin structure causing the copper site geometry to flatten slightly and the imidazole remote nitrogens to have different hydrogen-bonding interactions.

EXPERIMENTAL PROCEDURES

Porcine insulin was either purchased from Sigma or was generously donated by Eli Lilly Co. Crystals of 2Cu-insulin were grown by reported methods for the crystal growth of 2Zn-insulin (*28*), only replacing zinc sulfate with cupric sulfate. Crystals were grown by dissolving 50 mg of insulin in 5 mL of 0.2 M HCl and then adding in order 0.5 mL of 0.12 M copper sulfate, 2.5 mL of 0.2 M trisodium citrate, 1.5 mL of acetone, and 1.5 mL of water. The final solution pH was 6.2. Small, well formed crystals developed in filtered solutions after 1−5 days and had morphologies consistent with those of 2Zn-insulin (*26*). Samples consisting of a slurry of well-defined crystals of varying size (up to ≈0.1 mm) were placed in EPR tubes. After the crystals were allowed to settle, the mother liquors were pipetted out and 0.12 M sodium citrate was added several times to wash the crystals. For the Cd^{2+} binding studies, a modification of a procedure reported by Hill et al. (*31*) was used. Here, multicrystal Cu^{2+}-insulin samples were allowed to soak in 0.5 mL of 2−5 mM cadmium acetate for 10−12 h and then washed with 0.12 M sodium citrate. Samples were frozen in liquid N_2 (77 K).

EPR measurements were performed at 77 K employing a Varian E-112 X-band spectrometer. Three-pulse ESEEM decay envelopes were obtained at 4.2 K with a home-built X-band pulsed-EPR spectrometer, cavity and resonator, whose designs and operation have been described in previous work (*7, 32*). Postprocessing of the echo decay envelopes including fast Fourier transformation was performed with software previously described (*32, 33*). EPR simulations were performed with a version of the Program QPOW (*34*) modified by Cornelius et al. (*33*). ESEEM simulations were obtained using the program NANGSEL (*33*), which was based on modulation functions developed by Mims (*4, 35*). The NANGSEL version employed was modified to run on a SGI Indigo^2 workstation by Krystek (*36*). Protein structural modeling was accomplished by use of either home-written software or the program O (*37*). The 2Zn-insulin atomic

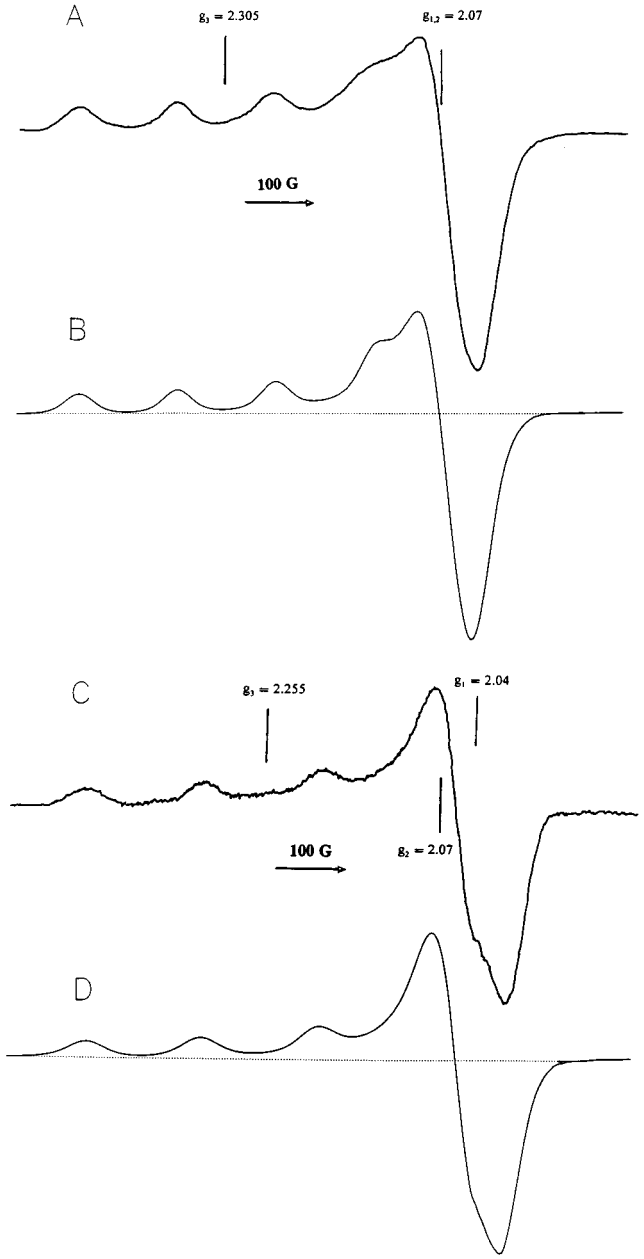

FIGURE 1: (A) X-band (9.2724 GHz) EPR spectrum of multicrystalline Cu^{2+}-insulin. Spectrum B is a simulation using the following parameters: $g_3 = 2.305$, $A_3^{Cu} = 158 \times 10^{-4}$ cm^{-1}, $g_1 = g_2 = 2.07$, $A_1^{Cu} = A_2^{Cu} = 0$ cm^{-1}, and a spectral line width of ≈20 G. (C) X-band (9.2589 Ghz) EPR spectrum of multicrystalline Cu^{2+}-insulin with added Cd^{2+}. Spectrum D is a simulation using the following parameters: $g_3 = 2.255$, $A_3^{Cu} = 178 \times 10^{-4}$ cm^{-1}, $g_1 = g_2 = 2.07$, $A_1^{Cu} = A_2^{Cu} = 0$ cm^{-1}, and a spectral line width of 20 G. The ESEEM experiments were carried out at a resonant field close to the g_2 region of the EPR spectrum, as this is where the electron spin−echo was at maximum intensity.

coordinates used in these calculations were those determined from a joint X-ray and neutron diffraction study (*38*) and obtained from a released entry (pdb3ins.ent) of the Protein Data Bank.

RESULTS

The EPR spectrum obtained for multicrystalline Cu^{2+}-insulin is shown in Figure 1A. Measured parameters are $g_3 = 2.305$, $A_3^{Cu} = 158 \times 10^{-4}$ cm^{-1}, $g_1 \approx g_2 = 2.07$, and $A_1^{Cu} \approx A_2^{Cu} = 0$ cm^{-1} and are employed in a simulation

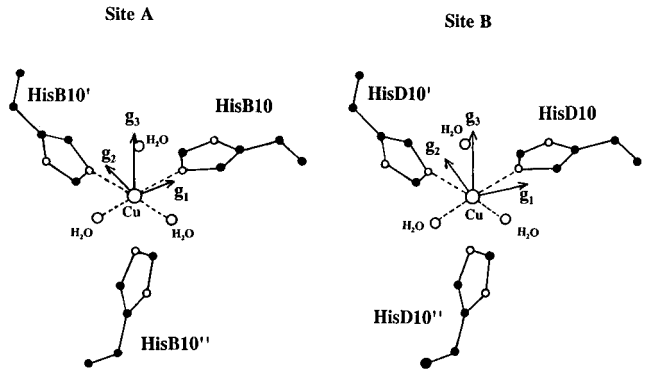

FIGURE 2: Schematic showing the two copper sites in Cu^{2+}-insulin and the relative orientations of the **g**-tensor directions with the ligand coordination.

depicted in Figure 1B. The spectrum is consistent with single-crystal parameters for 2Cu-insulin reported by Brill and Venable (*29*, *30*) (site I, $g_3 = 2.303$, $g_2 = 2.1$, $g_1 = 2.0$, and $A_3^{Cu} = 157 \times 10^{-4}$ cm^{-1}; site II, $g_3 = 2.304$, $g_2 = 2.10$, $g_1 = 2.00$, and $A_3^{Cu} = 159 \times 10^{-4}$ cm^{-1}) and also match the polycrystalline 2Cu-insulin EPR spectrum ($g_{||} = 2.308$, $A_{||}^{Cu} = 162 \times 10^{-4}$ cm^{-1}, $g_\perp = 2.07$, and $A_\perp^{Cu} = 0$ cm^{-1}) reported by Chasteen et al. (*39*).

At the time of Brill and Venable's single-crystal studies, the detailed structure of 2Zn-insulin was unknown and therefore no correlations could be made between the tensor principal directions and the zinc-substituted copper sites. It was necessary for the present analysis that such correlations be determined. The choice among various possibilities that relate the **g**-tensor to metal site geometry was made on the basis of the criterion that a minimum deviation be found between the $g_{||}$ principal direction and the normal to the best plane defined by the four approximate equatorial ligands. Such a criterion has been previously studied in light of both experimental and theoretical considerations (*40*, *41*) and has been found to be approximately valid even in systems that possess severe tetrahedral distortions (*41*). For 2Cu-insulin, the four equatorial ligands (Figure 2) correspond to the pair of Nϵ(His B10) and O(water 61), and another pair of Nϵ-(His B10′) and O(water 61′) related to the first by the 3-fold rotation axis for site A; and the pair of Nϵ(His D10) and O(water 272), and another pair of Nϵ(His D10′) and O(water 272′) related to the first by the 3-fold axis for site B. The best alignment of experimental g_3 directions derived from Brill and Venable (*29*) and the normal directions to the four roughly equatorial ligands were found to have angular deviations of ≈15° and ≈7° for copper sites A and B, respectively. In these correlations, the g_3 directions were also found to make angles of 2° and 15° with the axial Zn−Nϵ-(His B10″) and Zn−O(water 61″) directions, respectively, for site A and angles of 10° and 12° with the axial Zn−Nϵ-(His D10″) and Zn−O(water 272″) directions, respectively, for site B. In addition, for site A, the g_1 direction deviates from Cu−Nϵ(HisB10) by 22° and the g_2 direction deviates by 9° from Cu−Nϵ(HisB10′) and for site B, the g_1 direction deviates from Cu−Nϵ(HisD10) by 26° and the g_2 direction deviates by 40° from Cu−Nϵ(HisD10′). The relationship between **g**-tensors and copper (zinc) site geometries is shown in Figure 2.

The EPR spectrum of multicrystalline Cu^{2+}-insulin soaked in Cd^{2+} solution is depicted in Figure 1C. An EPR simulation

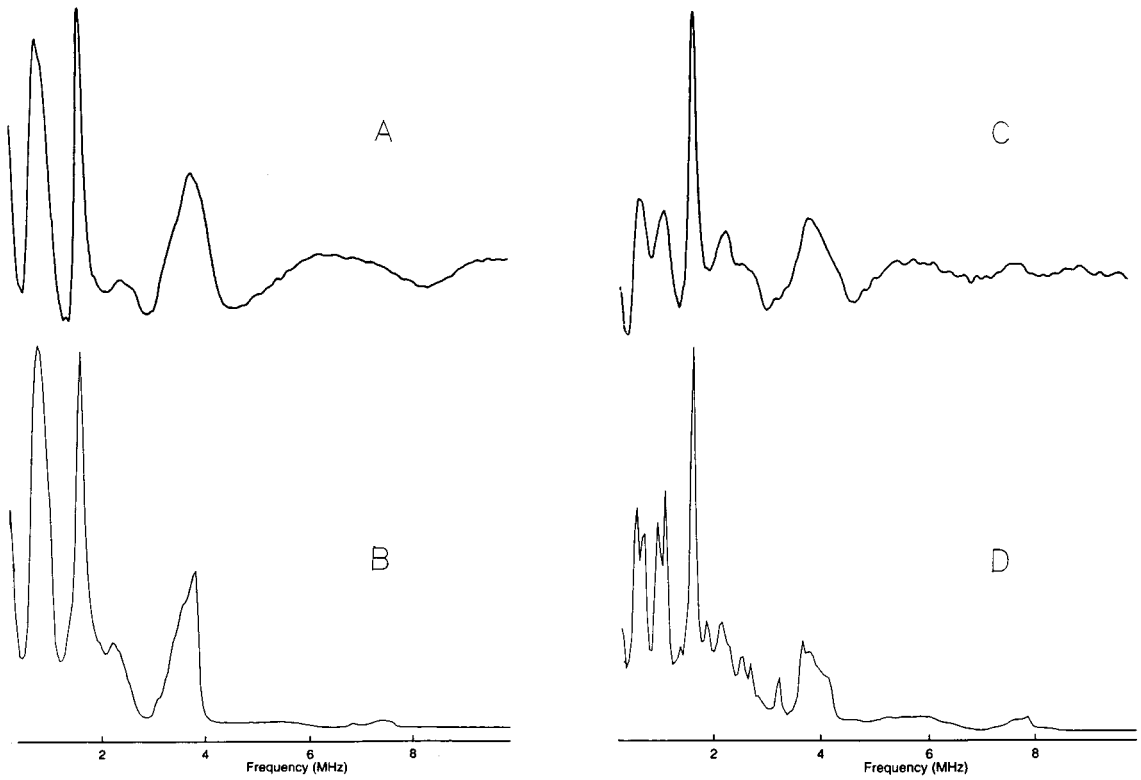

FIGURE 3: (A) FT-ESEEM spectrum of multicrystalline Cu^{2+}-insulin. The three-pulse experiment was carried out near $g = 2.07$ at a microwave frequency = 8.660 GHz, a field strength $H = 3005$ G, and an interpulse time, $\tau = 200$ ns. Trace B is a composite simulation for the two copper sites, employing the following parameters for both sites: $e^2qQ/h = -1.54$ MHz, $\eta = 0.90$, and $a_{iso} = 1.33$ MHz. The remaining hyperfine and quadrupole tensor parameters and alignments were assigned as discussed in the text. (C) ESEEM spectrum of multicrystalline Cu^{2+}-insulin with added Cd^{2+}. The three-pulse experiment was likewise carried out near $g = 2.07$ at a microwave frequency = 8.708 GHz, a field strength $H = 3010$ G, and an interpulse time, $\tau = 340$ ns. Trace D is a composite simulation for the two copper sites employing the following parameters; for copper site A, $e^2qQ/h = 1.67$ MHz, $\eta = 0.77$, and $a_{iso} = 1.68$ MHz; for copper site B, $e^2qQ/h = 1.76$ MHz, $\eta = 0.55$, and $a_{iso} = 1.68$ MHz. The remaining hyperfine and quadrupole tensor parameters and alignments were assigned as discussed in the text.

using parameters $g_3 = 2.255$, $A_3^{Cu} = 178 \times 10^{-4}$ cm^{-1}, $g_2 = 2.07$, $g_1 = 2.04$, and $A_1^{Cu} = A_2^{Cu} = 0$ cm^{-1} is displayed in Figure 1D. As compared to the spectra in Figure 1, the addition of Cd^{2+} causes g_3 to decrease from 2.305 to 2.255 and A_3^{Cu} to increase from 158×10^{-4} to 178×10^{-4} cm^{-1}. Also, the EPR signal intensity decreases to about 20% of its original value in Cu^{2+}-insulin. This is presumably because a significant amount of bound Cu^{2+} is replaced by Cd^{2+}, which is at a higher concentration. The observation of g and A^{Cu} shift is reversible. The original Cu^{2+}-insulin EPR signal is returned by allowing the Cd^{2+}-bound crystals to soak in a 0.12 M copper sulfate solution for a comparable time.

For Cu^{2+} complexes, a $g_{||}$ decrease concomitant with an $A_{||}^{Cu}$ increase is suggestive of a flattening of the coordination geometry toward a more planar arrangement, assuming identical ligand composition (*42, 43*). By use of results from Figures 1 and 3, a qualitative assessment of the amount of flattening may be made. Yokoi and Addison (*42*, Figure 6) plotted the dependence of $g_{||}$ on ω, the angle between chelate planes in a series of pyrrole-2-carboxaldehyde Schiff base copper complexes. If the copper exactly replaces zinc in the 2Zn-insulin structure, the angles between the ligand planes, (His)Nϵ−Cu−O(water) and (His)Nϵ−Cu−O(water), are calculated to be 60° and 68° for the A and B sites, respectively. Taken together with the g_3 values for Cu^{2+}-insulin, these parameters are found to nearly fit the $g_{||}$ versus ω curve of Yokoi and Addison (*42*). The g_3 value for Cu^{2+}-insulin with added Cd^{2+} then predicts that the copper coordination becomes more planar, or flatter, by ≈15° as compared to that found in the absence of Cd^{2+}.

The three-pulse ESE envelope modulation obtained for multicrystalline Cu^{2+}-insulin has characteristics typical for copper−imidazole complexes in proteins and small molecules (*2*). At X-band, the FT-ESEEM spectrum (Figure 3A) primarily consists of three lines from one electron spin manifold, two of which overlap near 0.75 MHz and a third, which is the sum of the lower two, near 1.5 MHz, and one broad line at 3.7 MHz arising from the other manifold. In addition, lines of low amplitude near 2.3 MHz are combination frequencies that arise from coupling of more than one nucleus (*32, 7*). A theoretical simulation of this spectrum is also shown in Figure 3B.

For Cu^{2+}-insulin, as found in many other copper proteins and copper−histidine model systems, the overlap of the two low-frequency lines (near 0.75 MHz in Figure 3A) signifies that the nqi asymmetry parameter, η, has a value near 0.9 (*8, 10*). The magnitudes of these three low frequencies, assuming the condition of "exact cancellation", are given by (*2, 10, 44*)

$$\nu_{\pm} = 3e^2qQ(1 \pm \eta/3)/4h$$

$$\nu_0 = e^2qQ\eta/2h$$

The broad line arising from the other spin manifold, at a frequency of 3.7 MHz, is largely dependent on the ^{14}N

hyperfine interaction and is approximately positioned (*2*) at

$$\nu_d = a_{iso} + 2\nu_n$$

Initial e^2qQ/h, η, and a_{iso} quantities were determined directly from the FT-ESEEM spectrum using these formulas.

Three parameters were adjusted to perform the final simulation. Since copper was presumed to replace the two zinc sites in the crystal, two of the histidine imidazoles for each site were taken as having orientations as found in the zinc structure. The g and A^{Cu} axes for both copper sites were aligned with the two zinc site coordinations as depicted in Figure 2. The remote nitrogen hyperfine anisotropy was assigned the values 0.38, −0.10, and −0.28 MHz, and tensors were oriented according to previous Cu^{2+}-doped histidine single-crystal models (*45*, *46*). The quadrupole tensor was positioned with respect to the imidazole bond geometries as found in the single-crystal ESEEM study of Cu(II)-doped bis(L-histidinato)Cd dihydrate (*46*), i.e., with e^2qQ/h directed normal to the imidazole plane. In addition, the two pairs of histidine imidazole remote nitrogens were considered to have equivalent couplings. This left only a_{iso} and the quadrupole parameters, e^2qQ/h and η, to be determined. The final ^{14}N tensor parameters employed in the simulation shown in Figure 3B are $e^2qQ/h = -1.54$ MHz, $\eta = 0.90$, and $a_{iso} = 1.33$ MHz, for both sites A and B.

The fit between simulated and experimental spectra is very good, except perhaps for the significantly larger broadening of the 3.7 MHz line in the experimental spectra. Three-pulse ESEEM experiments and simulations carried out at several other g-values of the EPR spectra were observed to have similar quality of fits. In some of these other FT-ESEEM spectra, the broad higher frequency line at 3.7 MHz in Figure 3A also exhibited small splittings in either the experiment or simulation. Various possibilities may give rise to this misfit, including the nonequivalence of the remote nitrogen couplings, the contribution of axially bound imidazole nitrogens (*33*), hyperfine anisotropies different than found in the model Cu^{2+}−histidine complexes, and an unaccounted-for reorientation of the histidine imidazoles upon copper substitution for zinc. However, any or all of these will not appreciably affect conclusions made below concerning the remote nitrogen quadrupole interactions.

The FT-ESEEM spectrum for cadmium-soaked crystalline samples is shown in Figure 3C. Modulation frequency lines at 0.56, 1.0, and 1.58 MHz from one electron manifold and at 3.81 MHz from the other are evident. In addition, preliminary ESEEM simulations identify the lines of lower amplitude near 2.2, 2.5, and 7.6 MHz as combination frequencies. For the simulation in Figure 3D, a similar procedure was followed as outlined above. The **g** tensor (and $\mathbf{A}^{Cu}$ tensor) orientations for both copper species were again placed in correspondence with the ligand geometry in the two zinc sites as reported in Figure 2. However, principal values from Figure 1C were employed. The ESEEM analysis here was found to be slightly more complicated. A closer examination of the spectrum in Figure 3C reveals a larger line width for the frequency lines at 0.56 and 1.0 MHz, as compared to other lines in the spectrum, as well as the appearance of a slight splitting of combination frequency lines near 2.5 MHz. Both these features arise from the nonequivalence of the quadrupole parameters of the nitrogens. Initial simulations were therefore performed as were described above but with different values of the e^2qQ/h and η for the nitrogens of each site. Further, the imidazole conformations were changed from those found in the native 2Zn-insulin crystal structure and fixed at specific orientations throughout these simulations for reasons and in a manner discussed below. Simulation trials using native imidazole orientations did not give as good a fit to the experimental observations. With these new imidazole orientations, ESEEM spectral simulations were calculated with the orientation of the nitrogens' quadrupole tensors similar to that found in the single-crystal ESEEM study of Cu^{2+}-doped l-histidine·HCl·H_2O (*45*), as this configuration was found to give a better correspondence to the experimental spectra. Here e^2qQ/h is directed in the imidazole plane and perpendicular to the N−H bond. Final FT-ESEEM simulations displayed in Figure 3D employed the following ^{14}N parameters: for site A, $e^2qQ/h = 1.67$ MHz, $\eta = 0.77$, and $a_{iso} = 1.68$ MHz; and for site B, $e^2qQ/h = 1.76$ MHz, $\eta = 0.55$, and $a_{iso} = 1.68$ MHz.

These ^{14}N parameters predict the experimental spectrum very well, but perhaps not as well as found for Cu^{2+}-insulin in the absence of Cd^{2+} (Figure 3B). Again there seems to be an unexplained broadening of all the experimental lines. Similar fits and results were found upon comparing experimental and simulated FT-ESEEM at other g-values of the EPR spectra. Various reasons have been specified above that may give rise to this broadening. An additional uncertainty arises from the probable reorientation of **g** tensors (and $\mathbf{A}^{Cu}$ tensors) axes with respect to the metal coordination geometry.

DISCUSSION

Brill and Venable found that the copper coordination in 2Cu-insulin is a distorted octahedron consisting of two histidine imidazoles and two water molecules positioned in an approximate equatorial plane, and a third water and histidine imidazole axially bound (*29*, *30*). The two copper atoms were believed to isomorphously substitute for the two zincs in the 2Zn-insulin structure, both sites undergoing a local Jahn−Teller distortion. Our ESEEM results are consistent with this conclusion. Although no strong evidence is found for axial imidazole nitrogen coordination, the ESEEM observations provide a confirmation that two histidine imidazoles ligate to copper in an approximate equatorial fashion in each site. In addition, simulations using the native imidazole coordinates closely match the observed spectra, suggesting that copper does indeed isomorphously replace zinc in the insulin structure.

EPR and ESEEM observations indicate that the insulin copper site undergoes a specific structural alteration when Cd^{2+} binds. A model for this alteration was formulated by rotating each of the imidazole moieties about their $C_\beta-C_\gamma$ bonds by ≈25°. This movement allows each imidazole to direct its $N_\delta-H$ bond almost directly toward an oxygen of a nearby glutamate (GluB13), whose side chain also realigns to accommodate the Cd^{2+} as discussed below. These side chains were postitioned according to a description in a report on the crystal structure of 3Cd-insulin (*31*).

The structure of 3Cd-insulin shows that, in addition to Cd^{2+} substituting for the Zn^{2+} ions, one Cd^{2+} coordinates to two of the six GluB13 side chains present at the hexamer

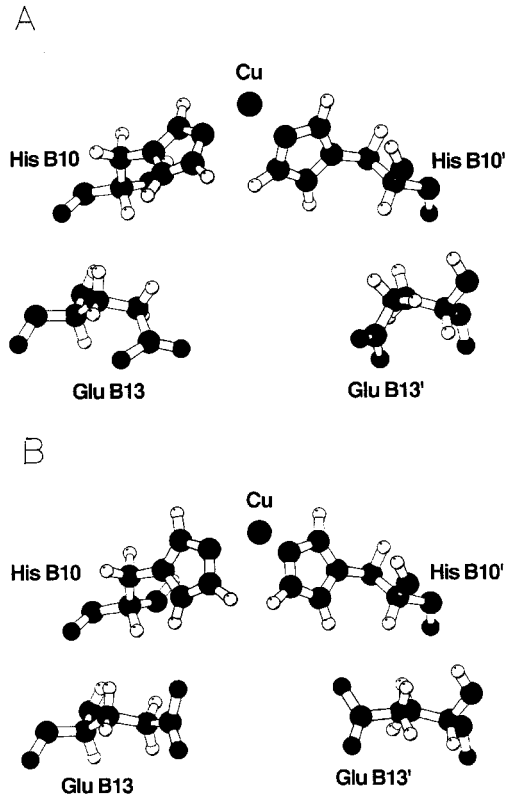

FIGURE 4: MOLSCRIPT (*47*) ball-and-stick images of the copper site A in Cu^{2+}-insulin showing the two equatorial coordinating histidines and two of the six close glutamates (GluB13) at the hexamer interface. Structure A shows orientations for these amino acids found in 2Zn-insulin by crystallography (*38*). Structure B depicts the altered positions of these glutamates to accommodate the binding of Cd^{2+} in 3Cd-insulin. In these reoriented positions, the glutamate side-chain oxygens are favorably aligned to hydrogen-bond to the remote nitrogen of the coordinated histidines, which have also been rotated about their C_β-C_γ bonds by about 25° from that found in the 2Zn-insulin structure.

interface, causing these to change conformation (*31*). However, because of the close proximity of the *c*-axis to the cadmium site, three potential cadmium sites are present, each having a metal occupancy of one-third. Hill et al. (*31*) mentioned that the Cd^{2+} ion, having equal probability to bind any two of the six glutamates, rapidly migrates from one site to the next. This presumably causes the glutamates to continuously adjust their conformation at room temperature.

The cadmium-bound glutamate side chains shown in Figure 9 of Hill et al. (*31*) have their Oϵ oxygens in favorable alignments to hydrogen bond with the remote Nϵ nitrogens of the B10 histidines, provided the imidazole moieties also rotate slightly about their $C_\beta-C_\gamma$ bond. It is proposed that in Cu^{2+}-insulin the binding of cadmium causes the glutamate side-chain oxygens to form hydrogen-bonding interactions with the B10 histidine remote nitrogens, locking these conformations into place. The copper concomitantly relaxes to a more planar geometry as shown by the EPR, allowing the imidazoles to rotate slightly to further stabilize the imidazole−glutamate interactions and the copper site. ESEEM spectral simulations with the imidazoles in these new reoriented positions have been shown above to correspond very well with the experimental spectra. Figure 4 depicts a MOLSCRIPT (*47*) illustration of the copper site A with the coordinated B10 histidines and the B13 glutamates in orientations found in 2Zn-insulin (Figure 4A) and with rotated conformations of these histidines modeled to hydrogen-bond to the nearby reoriented glutamates (Figure 4B).

The maximum quadrupole interaction $|e^2qQ/h|$ for the remote nitrogen is observed to change direction from along the imidazole plane normal in Cu-insulin to an in-plane alignment in Cd^{2+}-soaked samples. Previous studies on copper-doped histidine single-crystal models indicated that a 90° rotation of $|e^2qQ/h|$ to an in-plane direction signifies a lower N−H orbital occupancy for the imidazole remote nitrogens, which may be a reflection of the presence of a stronger hydrogen-bonding interaction (*45*, *46*).

Precise nqi parameters for two histidine imidazole nitrogens in a copper protein were also obtained recently from pulsed-ENDOR and ESEEM studies on single crystals of the blue copper protein azurin (*11*, *56*). The orientations of the coupling tensor principal axes of the remote nitrogens corresponded to those obtained from Cu^{2+}-histidine single-crystal model systems (*45*, *46*), and therefore a definitive assignment was made concerning the origin of the observed interactions. The azurin His117 Nϵ nitrogen, which is hydrogen-bonded to water (OW137), was found to have nqi parameters of $|e^2qQ/h| = 1.43$ MHz and $\eta = 0.95$, whereas the His46 Nϵ nitrogen, hydrogen-bonded to O of Asn10, had reported parameters of $|e^2qQ/h| = 1.37$ MHz and $\eta = 0.86$ (*11*). The azurin copper site is structurally very asymmetric, posessing different interactions with the two imidazole ligands (*12*). Because of this, the magnitudes of the hyperfine parameters for the two remote nitrogens were also found to be significantly different from each other and appeared to scale by an amount that could be attributed to the unequal spin distribution on the imidazole ligands (*11*). This structural inequivalence between the two histidines, however, also makes it difficult to unambiguously establish the origin of the remote ^{14}N nqi differences.

The combined results from Cu^{2+}-insulin and azurin demonstrate that when the histidine imidazole remote nitrogen hydrogen bonds to a water molecule, the nqi parameters possess similar values; $|e^2qQ/h| \approx 1.4$ MHz and $\eta \approx 0.92$. This suggests and lends credence to the hypothesis that the hydrogen-bonding environment is the dominant determinant of the variations observed in the nqi parameters in histidine imidazole.

Table 1 lists results from selected ESEEM investigations of copper proteins, including two Cu^{2+}-doped histidine model systems, and the associated known crystal structures. A comparison of the coordinated imidazole remote ^{14}N nqi parameters with the hydrogen-bonding environments reveals that a large η ($\eta \geq 0.9$) is observed whenever the histidine imidazole remote nitrogen is hydrogen bonded to water, irrespective of whether this nitrogen is Nδ or Nϵ. Conversely, a smaller η ($0.65 < \eta < 0.9$) is observed whenever either remote nitrogen, Nδ or Nϵ, makes a hydrogen bond to the protein or, in the case of histidine model systems, to a carboxylate oxygen. The e^2qQ/h parameter varies from 1.37 to 1.70 MHz but does not appear to depend on the nature of the remote nitrogen or on the hydrogen-bond acceptor.

CONCLUSIONS

ESEEM spectroscopy was used to determine the ^{14}N hyperfine and quadrupole coupling parameters for the remote nitrogen of two equatorially coordinated histidine imidazoles

Table 1: Comparison of the ^{14}N Nqi Parameters Determined by Pulsed-EPR Studies[a] with the Coordinated Imidazole Remote Nitrogen Hydrogen-Bonding Environments Determined by Diffraction Experiments[b] for Selected Copper Proteins and Doped Single-Crystal Models[c]

system	sample	His	H-bond	η	$\lvert e^2qQ/h \rvert$ (MHz)
		Protein			
lactoferrin	frozen soln	His253	Nδ- -OW3	0.9	1.6
		His597	Nδ- -OW93	0.9	1.6
stellacyanin	frozen soln	His46	Nϵ- -OW179	0.90	
		His94	Nϵ- -OW125	0.90	
insulin	multicrystal site A	HisB10	Nδ- -OW62	0.90	1.54
		HisB10′	Nδ- -OW62′	0.90	1.54
	multicrystal site B	HisD10	Nδ- -OW702	0.90	1.54
		HisD10′	Nδ- -OW702′	0.90	1.54
azurin	single crystal	His117	Nϵ- -OW137	0.95	1.43
		His46	Nϵ- -OAsn10	0.86	1.37
galactose oxidase	frozen soln	His496	Nδ- -OGly513	0.65	1.70
		His581	Nδ- -OThy580	0.65	1.70
		Model Single Crystal			
Cu(II)-histidine·HCl·H_2O		His	Nδ- -OHis	0.66	1.40
Cu(II)-bis(L-histidinato)Cd·H_2O		His	Nϵ- -OHis	0.65	1.56

[a] The pulsed-EPR results were obtained from the following investigations: for lactoferrin (*60*), for stellacyanin (*57, 58*), for insulin (the present work), for azurin (*11*), for galactose oxidase (*10, 61*), for Cu^{2+}-doped L-histidine·HCl·H_2O (*45*), and for Cu^{2+}-doped bis(L-histidinato)Cd·H_2O (*46*). [b] The X-ray or neutron diffraction results were obtained from the following investigations: for lactoferrin (*58*), for stellacyanin (*22*), for insulin (*28*), for azurin (*12*), for galactose oxidase (*49*), for Cu^{2+}-doped L-histidine·HCl·H_2O (*62*), and for Cu^{2+}-doped bis(l-histidinato)Cd·H_2O (*63*). [c] Crystallographic results from these systems reveal that the imidazole remote nitrogen of the coordinated histidines exclusively forms a hydrogen bond either to the oxygen of a water or to an amino acid. In *Cucumis sativus* stellacyanin, the FT-ESEEM spectra has been reported without a detailed analysis (*56*). However, the almost exact coincidence of the spectral lines below 2 MHz of the ESEEM spectrum with that published for *Rhus vernicifera* stellacyanin, where a detailed analysis has been accomplished (*58*), implies similar nqi parameters exist for these two proteins. The η value (0.90) obtained from *Rhus vernicifera* stellacyanin for the remote nitrogens (*58*) has therefore been entered in Table 1 for *Cucumis sativus* stellacyanin. In Cu^{2+}-insulin, the primed histidines and waters represent molecules related by the crystallographic 3-fold axis. The Cu^{2+}-insulin structure has been assumed to be identical to that of 2Zn-insulin. In Cu^{2+}-substituted human lactoferrin, two metal sites exist, each with one histidine coordinating the copper ion (*59*).

in Cu^{2+}-substituted 2Zn-insulin. In the native 2Zn-insulin crystal structure, these nitrogens are hydrogen-bonded to water molecules (*28*). The excellent fit of FT-ESEEM simulations to experiments using imidazole orientations found in the native 2Zn-insulin crystal structure indicates that little alteration in metal coordination geometry occurs when Cu^{2+} substitutes for Zn^{2+}. This work thus provides a first determination of nqi parameters of an imidazole remote Nδ in a type 2 copper site where there is some assurance that this nitrogen has maintained its hydrogen bond to a water molecule.

When Cd^{2+} binds to the Cu^{2+}-insulin structure, a significant change takes place in both the EPR and ESEEM patterns. Spectral analysis shows that the histidine imidazoles form a stronger hydrogen bond to those glutamate residues that are responsible for the binding of cadmium. This work thus demonstrates for the first time a dependence of the remote nitrogen nqi on a specific structural alteration in a protein system.

The observation of similar nqi parameters for remote nitrogens hydrogen-bonded to water in both crystalline azurin and insulin is consistent with the view that the type of hydrogen-bonding interactions are the primary cause of observed differences for these parameters in copper proteins. Results derived from both pulsed-EPR and diffraction studies show that when the imidazole remote nitrogen hydrogen-bonds to water, η is most likely larger than or equal to 0.9, and when it makes a hydrogen bond to the protein, η is smaller than 0.9. This trend has potential in obtaining structural information at the metal site in structurally uncharacterized metalloproteins by pulsed-EPR methods.

ACKNOWLEDGMENT

We gratefully acknowledge the gift of porcine insulin from Eli Lilly and Company.

REFERENCES

1. Mims, W. B., and Peisach, J. (1976) *Biochemistry 15*, 3863−3869.
2. Mims, W. B., and Peisach, J. (1978) *J. Chem. Phys. 69*, 4921−4930.
3. Flanagan, H. L., and Singel, D. J. (1987) *J. Chem. Phys. 87*, 5606−5616.
4. Mims, W. B. (1972) *Phys. Rev. B7*, 2409−2419.
5. Dikanov, S. A., Shubin, A. A., and Parmon, V. N. (1981) *J. Magn. Reson. 42*, 474−487.
6. McCracken, J., Pember, S., Benkovic, S. J., Villafranca, J. J., Miller, R. J., and Peisach, J. (1988) *J. Am. Chem. Soc. 110*, 1069−1074.
7. Bender, C. J., Casimiro, D. R., Peisach, J., and Dyson, H. J. (1997) *J. Chem. Soc., Faraday Trans. 93*, 3967−3980.
8. Peisach, J. (1995) in *Bioradicals Detected by ESR Spectroscopy* (Ohya-Nishiguchi, H., and Packer, L., Eds.) pp 203−215, Birkhauser Verlag, Basel, Switzerland.
9. Avigliano, L., Davis, J. L., Graziani, M. T., Marchesini, A., Mims, W. B., Mondovi, B., and Peisach, J. (1991) *FEBS Lett. 136*, 80−84.
10. Jiang, F., McCracken, J., and Peisach, J. (1990) *J. Am. Chem. Soc. 112*, 9035−9044.
11. Coremans, J. A. W., Poluektov, O. G., Goenen, E. J. J., Canters, G. W., Nar, H., and Messerchmidt, A. A. (1996) *J. Am. Chem. Soc. 118*, 12141−12153.
12. Baker, E. N. (1988) *J. Mol. Biol. 203*, 1071−1095.
13. Petratos, K., Dauter, Z., and Wilson, K. S. (1988) *Acta Crystallogr. B44*, 628−636.
14. Guss, J. M., Bartunik, H. D., and Freeman, H. C. (1992) *Acta Crystallogr. B48*, 790−811.

15. Messerschmidt, A., Ladenstein, R., Huber, R., Bolognesi, M., Avigliano, L., Petruzelli, R., Rossi, A., and Finazzi-Agro, A. (1992) *J. Mol. Biol. 224*, 179−205.
16. Romero, A., Nar, H., Huber, R., Messerschmidt, A., Kalverda, A., Canters, G. W., Durley, R., and Mathews, F. S. (1994) *J. Mol. Biol. 236*, 1196−1211.
17. Guss, J. M., Meritt, E. A., Phizackerley, R. P., and Freeman, H. C. (1996) *J. Mol. Biol. 262*, 686−705.
18. Walter, R. L., Ealick, S. E., Friedman, A. M., Blake, R. C., II, Proctor, P., and Shoham, M. (1996) *J. Mol. Biol. 263*, 730−751.
19. Xue, Y., Okvist, M., Hansson, O., and Young, S. (1998) *Protein Sci. 7*, 2099−3105.
20. Ducros, V., Brzozowski, A. M., Wilson, K. S., Brown, S. H., Ostergaard, P., Schneider, P., Yaver, D. S., Pedersen, A. H., and Davies, G. H. (1998) *Nat. Struct. Biol. 5*, 310−316.
21. Bond, C. S., Bendall, D. S., Freeman, H. C., Guss, J. M., Howe, C. J., Wagner, M. J., and Wilce, M. C. (1999) *Acta Crystallogr. D55*, 414−421.
22. Hart, P. J., Nersissian, A. M., Herrmann, R. G., Nalbandyan, R. M., Valentine, J. S., and Eisenberg, D. (1996) *Protein Sci. 5*, 2175−2183.
23. Nar, H., Messerschmidt, A., Huber, R., van de Kamp, M., and Canters, G. W. (1991) *J. Mol. Biol. 218*, 427−447.
24. Mathews, C. K., and van Holde, K. E. (1990) *Biochemistry* Benjamin/Cummings, Menlo Park, CA.
25. Schlichtkrull, J. (1956) *Acta Chem. Scand. 10*, 1455−1458.
26. Schlichtkrull, J. (1958) *Insulin Crystals*, Ejnar Munksgaard, Copenhagen, Denmark.
27. Blundell, F. R. S., T. L., Dodson, G. G., Hodgkin, F. R. S., D. M. C., and Mercola, D. A. (1972) *Adv. Protein Chem. 26*, 279−402.
28. Baker, E. N., Blundell, F. R. S., T. L., Cutfield, J. F., Cutfield, S. M., Dodson, E. J., Dodson, G. G., Hodgkin, F. R. S., D. M. C., Hubbard, R. E., Issacs, N. W., Reynolds, C. D., Sakabe, K., Sakabe, N., and Vijayan, N. M. (1988) *Philos. Trans. R. Soc. London B319*, 369−456.
29. Brill, A. S., and Venable, J. H., Jr. (1968) *J. Mol. Biol. 36*, 343−353.
30. Brill, A. S., and Venable, J. H., Jr. (1972) *J. Mol. Biol. 66*, 169−180.
31. Hill, C. P., Dauter, Z., Dodson, E. J., Dodson, G. G., and Dunn, M. F. (1991) *Biochemistry 30*, 917−924.
32. McCracken, J., Peisach, J., and Dooley, D. M. (1987) *J. Am. Chem. Soc. 109*, 4064−4072.
33. Cornelius, J. B., McCracken, J., Clarkson, R. B., Belford, R. L., and Peisach, J. (1990) *J. Phys. Chem. 94*, 6977−6982.
34. (a) Belford, R. L., and Nigles, M. J. (1979) Computer simulation of powder spectra, at *EPR Symposium, 21st Rocky Mountain Conference*, Denver, CO. (b) Nigles, M. J. (1979) Ph.D. Thesis, University of Illinois, Urbana, IL. (c) Maurice, A. M. (1980) Ph.D. Thesis, University of Illinois, Urbana, IL.
35. Mims, W. B. (1972) *Phys. Rev. B6*, 3543−3545.
36. Krystek, J. (1995) Unpublished results.
37. Jones, T. A., Zou, J. Y., Cowan, S. W., and Kjeldgaard, M. (1991) *Acta Crystallogr. A47*, 110−119.
38. Wlodawer, A., Savage, H., and Dodson, G. (1989) *Acta Crystallogr. B45*, 99−107.
39. Chasteen, N. D., DeKoch, R. J., Rogers, B. L., and Hanna, M. W. (1972) *J. Am. Chem. Soc. 95*, 1301−1309.
40. Lieberman, R. A., Sands, R. H., and Fee, J. A. (1982) *J. Biol. Chem. 257*, 336−344.
41. Miyamoto, R., Ohba, Y., and Iwaizumi, M. (1992) *Inorg. Chem. 31*, 3138−3149.
42. Yokoi, H., and Addison, A. W. (1977) *Inorg. Chem. 16*, 1341−1349.
43. Sakaguchi, U., and Addison, A. W. (1977) *J. Am. Chem. Soc. 99*, 5189−5190.
44. Hunt, M. J., Mackay, B. R., and Edmonds, D. T. (1975) *Chem. Phys. Lett.*, 473−475.
45. Colaneri, M. J., and Peisach, J. (1992) *J. Am. Chem. Soc. 114*, 5335−5341.
46. Colaneri, M. J., and Peisach, J. (1995) *J. Am. Chem. Soc. 117*, 6308−6315.
47. Kraulis, P. J. (1991) *J. Appl. Crystallogr. 24*, 946−950.
48. Hirasawa, R., and Kon, H. (1972) *J. Chem. Phys. 56*, 4467−4474.
49. McDowell, C. A., Naito, A., Sastry, D. L., Cui, Y. U., Sha, K., and Yu, S. X. (1989) *J. Mol. Struct. 195*, 361−381.
50. Ito, N., Phillips, S. E. V., Stevens, C., Ogel, Z. B., McPherson, M. J., Keen, J. N., Yadav, K. D. S., and Knowles, P. F. (1991) *Nature 350*, 87−90.
51. Murphy, M. E., Turley, S., Kukimoto, M., Nishiyama, M., Horinouchi, S., Sasaki, H., Tanokura, M., and Adman, E. T. (1995) *Biochemistry 34*, 12107−12117.
52. Adman, E. T., Godden, J. W., and Turley, S. (1995) *J. Mol. Biol. 46*, 27458−27474.
53. Kumar, V., Dooley, D. M., Freeman, H. C., Guss, J. M., Harvey, I., McGuirl, M. A., Wilce, M. C., and Zubak, V. M. (1996) *Structure 4*, 943−955.
54. Wilce, M. C., Dooley, D. M., Freeman, H. C., Guss, J. M., Matsunami, H., Mcintire, W. S., Ruggiero, C. E., Tanizawa, K., and Yamaguchi, H. (1997) *Biochemistry 36*, 16116−11133.
55. Adman, E. T. (1985) *Top. Mol. Struct. Biol. 6*, 1−42.
56. Coremans, J. A. W., Poluektov, O. G., Goenen, E. J. J., Canters, G. W., Nar, H., and Messerchmidt, A. A. (1997) *J. Am. Chem. Soc. 119*, 4726−4731.
57. Nersissian, A. M., Mehrabian, Z. B., Nalbandyan, R. M., Hart, P. J., Fraczkiewicz, G., Czernuszewicz, R. S., Bender, C. J., Peisach, J., Herrmann, R. G., and Valentine, J. S. (1996) *Protein Sci. 5*, 2184−2192.
58. Bender, C. J.. and Peisach, J. (1998) *J. Chem. Soc., Faraday Trans. 94*, 375−386.
59. Smith, C. A., Anderson, B. F., Baker, H. M., and Baker, E. N. (1992) *Biochemistry 31*, 4527−4533.
60. Eaton, S. S., Dubach, J., More, K. M., Eaton, G. R., Thurman, G., and Ambruso, D. R. (1989) *J. Biol. Chem. 264*, 4776−4781.
61. Kosman, D. J., Peisach, J., and Mims, W. B. (1980) *Biochemistry 19*, 1304−1308.
62. Fuess, H., Hohlwein, D., and Mason, S. A. (1997) *Acta Crystallogr. B33*, 654−658.
63. Fuess, H., and Bartunick, H. (1976) *Acta Crystallogr. B32*, 2803−2806.

BI991613V